NeuroImage 202 (2019) 116141

Contents lists available at ScienceDirect

NeuroImage

journal homepage: www.elsevier.com/locate/neuroimage

Retrospective motion compensation for edited MR spectroscopic imaging

Kimberly L. Chan [a,*], Peter B. Barker [b,c]

[a] Advanced Imaging Research Center, University of Texas Southwestern Medical Center, Dallas, TX, USA
[b] Russell H. Morgan Department of Radiology and Radiological Science, The Johns Hopkins University School of Medicine, Baltimore, MD, USA
[c] F. M. Kirby Research Center for Functional Brain Imaging, Kennedy Krieger Institute, Baltimore, MD, USA

ARTICLE INFO

Keywords:
Editing
GABA
GSH
MEGA-PRESS
MRS
MRSI
Brain

ABSTRACT

Edited magnetic resonance spectroscopic imaging (MRSI) is capable of mapping the distribution of low concentration metabolites such as gamma-aminobutyric acid (GABA) or and glutathione (GSH), but is prone to subtraction artifacts due to head motion or other instabilities. In this study, a retrospective motion compensation algorithm for edited MRSI is proposed. The algorithm identifies movement-affected signals by comparing residual water and lipid peaks between different transients recorded at the same point in k-space, and either phase corrects, replaces or removes affected spectra prior to spatial Fourier transformation. The method was tested on macromolecule-unsuppressed GABA-edited spin-echo MR spectroscopic imaging data acquired from 8 healthy adults scanned at 3T. Relative to non-motion compensated data sets, the motion compensated data had significantly less subtraction artifacts across subjects. The residual choline (Cho) peak in the spectrum (which is well resolved from as a different chemical shift from GABA and is completely absent in a spectrum without subtraction artifact) was used as a metric of motion artifact severity. The normalized Cho area was 5.14 times lower with motion compensation than without motion compensation. A 'removal-only' version of the technique is also shown to be promising in removing motion-corrupted artifacts in a GSH-edited MRSI acquisition acquired in 1 healthy subject. This study introduces a motion compensation technique and demonstrates that retrospective compensation in k-space is possible and significantly reduces the amount of subtraction artifacts in the resulting edited spectra.

1. Introduction

Edited proton MR spectroscopy (MRS) of the human brain at 3T is increasingly being used to detect lower-concentration compounds such as gamma-aminobutyric acid (GABA) or glutathione (GSH). GABA is the principle inhibitory neurotransmitter (Puts and Edden, 2012) and GSH is the brain's main antioxidant (Mytilineou et al., 2002). Both metabolites have also been implicated in a large range of neurological disorders and neuropsychiatric disorders (Schulz et al., 2000; Wood et al., 2009; Weiduschat et al., 2014; Mao et al., 2017; Petroff, 2002; Shetty and Bates, 2016; Do et al., 2018; Chang et al., 2003) and have been of interest in basic neuroscience (Dharmadhikari et al., 2015; Jocham et al., 2012; Isaacson and Scanziani, 2011). A variety of spectral editing techniques have been proposed based on either multiple-quantum filtering (Puts and Edden, 2012; Choi et al., 2009; Trabesinger et al., 1999) or J-difference editing (Puts and Edden, 2012; Edden et al., 2006; Matsuzawa et al., 2008; Chan et al., 2017; Harris et al., 2017). Of these two techniques, J-difference editing is the more widely used, most often in conjunction with single-voxel localization. However, in many cases it is desirable to detect spectra from multiple regions of interest, in order to map out spatial variations in metabolite levels. While single-voxel pulse sequences are useful if it is desirable to probe a specific region of interest, multi-voxel techniques are needed in situations where the affected area is unknown or if several areas are of interest. J-difference editing has been used in combination with MR spectroscopic imaging (MRSI) for multi-voxel localization and has previously been shown to be capable of mapping both GABA (Chan et al., 2019; Zhu et al., 2011; Bogner et al., 2014a) and GSH (Chan et al., 2019; Srinivasan et al., 2010).

Since J-difference editing involves the subtraction of two scans with and without editing pulses applied (referred to as ON and OFF respectively), it is very sensitive to head motion or other instabilities which cause subtraction artifacts (Bogner et al., 2014a; Evans et al., 2013). In single-voxel spectral editing, various post-processing schemes are available to identify and correct shot-to-shot phase and frequency variations (Mullins et al., 2014; Waddell et al., 2007; Near et al., 2015). These have been shown to remove subtraction artifacts and improve spectral quality.

* Corresponding author. Advanced Imaging Research Center, UT Southwestern Medical Center, 5323 Harry Hines Boulevard, NE.4.112, Dallas, TX 75390, USA.
E-mail address: kimberly.chan@utsouthwestern.edu (K.L. Chan).

https://doi.org/10.1016/j.neuroimage.2019.116141
Received 18 April 2019; Received in revised form 23 August 2019; Accepted 28 August 2019
Available online 31 August 2019

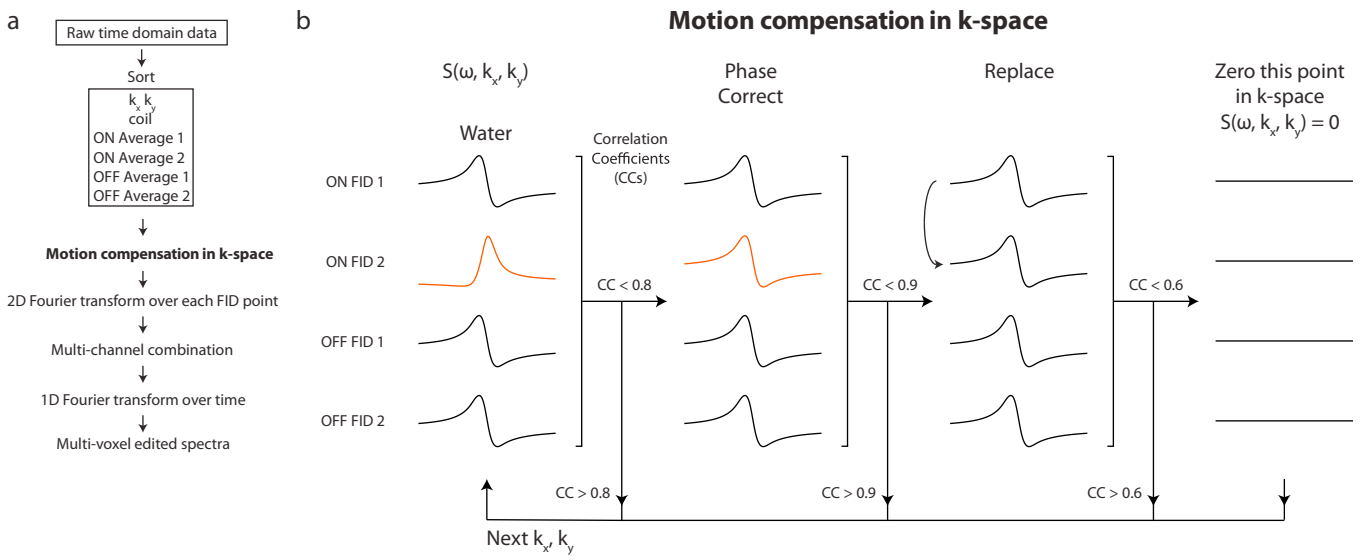

Fig. 1. (a) General schematic diagram of the edited MR spectroscopic imaging data processing pipeline including the retrospective motion compensation algorithm in k-space. (b) Motion-affected transients are identified depending on their correlation coefficients with the spectra at the same k-space point and are either phased to match the unaffected transients, replaced with an unaffected transient of the same type of sub-acquisition, or replaced by zeroes. For clarity purposes, only the water peak is displayed.

However, in edited MRSI, the presence of phase-encoding gradients has generally precluded application of such routines although prospective motion schemes with additional hardware and/or specialized software have been implemented for use with edited MRSI (Bogner et al., 2014b).

Motion-related corruption of even just a few points in k-space then leads to measurement biases which propagate throughout the entire MRSI dataset after spatial fast Fourier transformation (FFT). If the measurement bias differs between ON and OFF acquisitions, subtraction artifacts (i.e. the presence of unwanted signals) will occur. This can lead to mis-estimation and variability in the measurement of edited resonances due to overlap with subtraction artifacts.

In this paper, a retrospective motion compensation method for edited MR spectroscopic imaging is presented and evaluated on data acquired using a previously described pulse sequence for edited MRSI (Zhu et al., 2011). This sequence compares residual water and lipid peaks between different transients acquired at the same point in k-space, and either phase corrects, replaces or removes those that do not share the same properties as the others. After correction in k-space, data are processed as normal by spatial FFT. The algorithm is designed to work with datasets that contain only a limited amount of motion, i.e. the majority of the data being of good quality with only occasional head motion followed by a return to the original position. The method is not designed to compensate for larger or more continuous motion, in which case only prospective motion correction schemes (e.g. (Bogner et al., 2014b)) would be expected to be successful.

2. Materials and methods

2.1. Retrospective motion compensation scheme

In MRSI, the phase of the signal changes from one point in k-space to the next, so correction schemes developed for single voxel MRS will not work as applied to the whole dataset. However, if more than one transient is acquired for each point in k-space, then different transients at the same point in k-space can be compared for similarity. The pulse sequence used in this study (see below) gives quite strong residual water and lipid signals, which can be used to estimate motion-related phase, frequency or amplitude changes. It may also be possible to compare k-space spectra between acquisitions with the editing pulse either ON and OFF; for instance, in editing for GABA+, the water peak will usually be the same in both the ON and OFF spectra, so can also be compared for similarity, whereas the lipid peaks are usually affected by the 1.9 ppm ON GABA + editing, so cannot be compared.

Fig. 1 shows the general schematic of the entire data processing pipeline including the added motion compensation in k-space before 2D spatial FFT. The motion compensation algorithm, is based on the assumption that at least two transients at the same k-space point have similar phases then they are un-affected by motion. On the other hand, if a transient has a different phase from the others, it is assumed that it is motion-affected. To determine similarity between transients at the same k-space point, Pearson's correlation coefficients (CC) were calculated for the real parts of the water peaks (4.4 ppm–5.2 ppm) and lipid peaks (0 ppm–2.5 ppm) separately (Tapper et al., 2019; Wiegers et al., 2017) between all four transients to generate six CCs per point in k-space: $CC_{ON1,ON2}$, $CC_{ON1,OFF1}$, $CC_{ON1,OFF2}$, $CC_{ON2,OFF1}$, $CC_{ON2,OFF2}$, and $CC_{OFF1,OFF2}$. Since the lipid peaks differed between the ON and the OFF spectra, the lipid CCs were only calculated between transients of the same sub-acquisition type. Thus, the CCs can be defined as:

$$CC_{ON1,ON2} = CC_{water,ON1,ON2} \vee CC_{lipid,ON1,ON2}$$

$$CC_{ON1,OFF1} = CC_{water,ON1,OFF1}$$

$$CC_{ON1,OFF2} = CC_{water,ON1,OFF2}$$

$$CC_{ON2,OFF1} = CC_{water,ON2,OFF1}$$

$$CC_{ON2,OFF2} = CC_{water,ON2,OFF2}$$

$$CC_{OFF1,OFF2} = CC_{water,OFF1,ON2} \vee CC_{lipid,OFF1,OFF2}$$

Note that the lipid spectra are only included when finding the CCs between the ON transients and the OFF transients. After calculating the CCs between transients, the algorithm then determines which transients are affected by motion by determining which of the six CCs have values below a threshold of 0.8. Depending on the combination of CCs that have values below this threshold, the motion affected transient(s) can be surmised. For example if $CC_{ON1,ON2}$, $CC_{ON1,OFF1}$, $CC_{ON1,OFF2}$ are all below 0.8, it can be inferred that ON transient 1 is the motion-affected transient as that transient is shared between the CCs with values below the thresholds. Another example is if $CC_{ON1,OFF1}$, $CC_{ON2,OFF1}$, $CC_{ON2,OFF2}$ are all below 0.8. In this case, the algorithm sees that ON transient 2 and OFF transient 1 appear in 2 out of the 3 CCs below threshold and are thus

considered the motion-affected transient. At times, however, ambiguity can exist as to which of the transients are motion affected. To narrow down the motion-affected transients, $CC_{ON1,\ ON2}$ and $CC_{OFF1,\ OFF2}$ were recalculated to be the average of the water and lipid CCs. The following general rules were then applied:

1. If there is ambiguity over which of two transients is motion affected, the algorithm sums the CCs for each transient separately and finds which of the two transient has the higher (lower) sum CC. The transient with the lowest sum CC is deemed the motion-affected transient. For example, if only $CC_{OFF1,OFF2}$ is below the threshold, it is unclear as to whether OFF transient 1 or OFF transient 2 is the motion-affected transient. Thus, non-motion affected transients can be found with the equation: $\mathrm{argmax}(CC_{ON1,OFF1}+CC_{ON2,OFF1}, CC_{ON1,OFF2}+CC_{ON2,OFF2})$ If this equation is equal to 1, then it can be surmised that OFF transient 2 is the motion-affected transient. Conversely, if the equation is equal 2, then OFF transient 1 is the motion-affected transient.
2. Ambiguity can also arise when trying to identify ON/OFF pairs spared from motion-related phase changes. In these instances, the algorithm identifies the CC between different ON/OFF combinations with the highest value and considers the other two ON/OFF transients to be motion-affected. For example, if $CC_{ON1,ON2}$, $CC_{ON2,OFF1,}$ and $CC_{OFF1,\ OFF2}$ are all below threshold, it is difficult to determine which ON/OFF is motion-affected. This can be narrowed down with the following equation: $\mathrm{argmax}(CC_{ON1,OFF1}, CC_{ON2,OFF1}, CC_{ON2,OFF2})$ If this equation is equal to 1, 2, or 3 then it can be surmised that ON transient 2 and OFF transient 2, ON transient 1 and OFF transient 2, or ON transient 1 and OFF transient 1 respectively are the motion-affected transients.

After identifying motion-affected transients, a decision was made as to what to do with these motion-affected transients. If all six CCs were below a threshold of 0.6, the k-space point was replaced with zeros. If not, however, an attempt was made at applying a zero-order phase to the motion-affected transients so that the phase of the water peaks matched that of other transients as closely as possible. This was done by applying 360 degrees of phase at 1° increments to the motion-affected transients and recalculating the CCs between the individual motion-affected transients and the average non-motion-affected transients at each increment. If a CC of 0.9 and above was obtained between the water peaks of the phased motion-affected spectra and the motion-unaffected spectra, the phase that was used to correct the spectra was saved for later use. If it was not possible to obtain a CC of 0.9 and above by phasing the motion-affected spectra, the transient was marked for replacement by a transient of the same sub-acquisition type (e.g. replacing OFF transient 1 with OFF transient 2). For more information, the MATLAB code for the algorithm is included as supplementary material.

After corrections are applied for each motion-affected transient in k-space, conventional post-processing steps (spatial 2D Fourier transformation, etc.) can be performed to create multi-voxel spectra.

The algorithm schematic presented in Fig. 1b was designed for a two-transient acquisition regime (two edit-ONs/edit-OFFs). There are times, however, where it is desirable to acquire additional transients. In such cases, the schematic presented in Fig. 1b can be extended. Thus, a more general method is proposed in supporting Fig. 1 and is illustrated schematically for a three-transient acquisition scheme. In this scheme, identification of motion-affected transients is forgoed in favor of a more blind approach where an attempt is made to phase-match all transients at the same k-space point to the ON/OFF transient pair at the same k-space point with the highest CC. If phase-matching of the transients to this pair of transients with a $CC > 0.9$ is not possible, the same replacement and k-space zeroing steps are taken.

2.2. In vivo data

All experiments were performed on an Achieva 3T scanner (Philips, Best, The Netherlands) equipped with a 32-channel head coil. Data were acquired in 8 healthy adults (6 male, age: 30 ± 7 years) using an edited, spin-echo MRSI sequence with hyper-geometric dual-band (HGDB) water and lipid suppression, and outer-volume lipid suppression, as described previously (Zhu et al., 2010, 2011). A single 20 mm thick axial slice placed just above the level of the ventricles was acquired with 2D phase encoding, field-of-view of 180 mm × 210 mm, 12 × 14 phase encoding matrix, and elliptical k-space sampling, resulting in a nominal in-plane resolution of 1.5 cm × 1.5 cm and voxel size of 4.5 cm^3. TR/TE was 2s/80 ms while the total acquisition time was 17.5 min. Two transients for each of the ON and OFF sub-acquisitions were acquired at each phase-encoding step. A frequency-modulated 90° excitation pulse with a bandwidth of 4.3 kHz and an amplitude-modulated 180° refocusing pulse with a bandwidth of 1.3 kHz were used as previously described (Henning et al., 2009). 20 ms sinc-gaussian editing pulses were used with a bandwidth of 62 Hz. For GABA-editing, these editing pulses were placed at 1.9 and 0.7 ppm in the ON and OFF acquisitions respectively. Note that these editing pulses partially invert the 1.7 ppm macromolecule (MM) peak (Henry et al., 2001) so that the 3 ppm signal detected contains components from MM in addition to GABA and is thus referred to here as GABA+.

GSH-edited data were also acquired in 1 healthy adult (male, age 26) with the same acquisition parameters, including TR and TE, as the GABA-edited acquisition. In this acquisition, however, the edit-ON pulse was placed at 4.56 ppm and the edit-OFF pulse was placed at 7.58 ppm.

B_0 field homogeneity was optimized using a field-map based 2nd-order shimming routine (Gruetter, 1993). Separate water unsuppressed references were also acquired with one transient and at the same field-of-view and resolution as the edited-MRSI scans for coil combination purposes.

Data were processed with and without the use of the retrospective motion compensation algorithm (Fig. 1). For GABA-editing, in the absence of any motion, there should be no residual signal at 3.2 ppm, i.e. the choline (Cho) peak should be completely removed and the edited peak at 3.0 ppm should only contain components from GABA and macromolecules. A measure of the subtraction artifact intensity can therefore be quantified by measuring the Cho signal in the difference spectra as it appears at a different chemical shift from GABA. Cho and GABA + peaks were therefore fit using lineshape models as described previously (Edden et al., 2014). To evaluate the goodness of the fits, the coefficient of determination was calculated between the fitted model values and spectra. Voxels that the algorithm was unable to fit or had a coefficient of determination (R^2) of less than 0.85 were not included in further analyses. In addition, voxels that were better fit by a single Gaussian model from 2.65 ppm to 3.6 ppm to the GABA + than the Cho + Cr model and/or with a R^2 of greater than 0.92 were considered to contain no Cho subtraction artifacts. The fitted Cho artifact areas from the DIFF spectra were normalized and were thus expressed as a fraction relative to the fitted Cho areas from the OFF spectra. Outliers were calculated as elements greater than 3 scaled median absolute deviations away from the median and were removed from further analyses.

In individual subjects, the GABA+ and GSH peaks in the uncorrected and the corrected spectra were fit with a single Gaussian peak, as were the H_2O peaks in the unsuppressed water spectra. The areas of the fitted peaks were extracted and the ratio between the edited signal areas and the unsuppressed water areas were mapped across the slice.

3. Results

The thresholds for the identification of motion-affected transients and

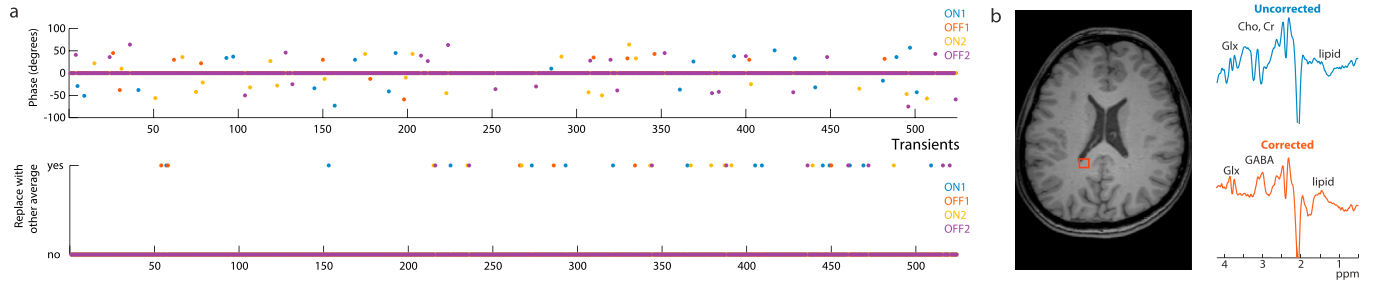

Fig. 2. (a) Phase corrections and transient replacements performed for one subject. A total number of 524 transients were acquired which is equal to $12 \times 14 \times 4$ (k_x, k_y, ON/OFF, 2 averages) *0.78 (elliptical k-space sampling). (b) Slice location for the edited MRSI acquisitions on an axial T_1-weighted image (middle) taken from the subject in (a). Representative uncorrected and corrected difference spectra from the subject in (a) from a voxel within this slice location are also shown plotted from 0.5 to 4.2 ppm. Negative Cho and Cr subtraction artifacts can be seen in the uncorrected data; these artifacts are removed after compensation and clear GABA+ and Glx peaks at 3.0 ppm and 3.75 ppm can be visualized in the corrected spectra.

cutoff for phase correction versus transient replacement was found after a parameter search ranging from 0.7 to 0.8 for motion-affected transient identification and 0.85 to 0.95 for the phase correction versus transient replacement cutoff. The optimal thresholds were chosen to minimize the residual Cho artifacts in the difference spectra while maximizing SNR. As shown in supporting Fig. 2, Cho artifacts across subjects were kept to a minimum with a threshold of 0.8 for motion-affected transient identification and 0.9 for phase correction. Fig. 2a shows the phase corrections and transient replacements made for a GABA-edited acquisition taken from one subject. Fig. 2b shows representative spectra taken from a voxel in one subject with and without the compensations depicted in Fig. 2a. It can be seen that there are significant artifacts which, in this case, manifest as predominantly negative Cho and Cr signals resulting from the magnitude of the OFF sub-acquisition being significantly greater than that of the ON sub-acquisition. With motion compensation, however, these subtraction artifacts are significantly reduced and clean GABA+ and glutamate + glutamine (Glx) peaks can be visualized at 3.0 and 3.7 ppm respectively. There is also less lipid contamination in the corrected spectra. A summary of all the phase corrections and transient replacements made can be seen in Table 1. Examples of curve-fitting of examples OFF and difference spectra from one subject are shown in supporting Fig. 3.

Fig. 3 shows the median distribution and interquartile range of the Cho artifacts across all 8 subjects represented as a fraction of the voxels fit inside the brain (average ± standard deviation of 128 ± 23 voxels). It can be seen that the Cho artifact distribution is skewed towards lower values in the corrected spectra versus the uncorrected spectra. This is also reflected in their median Cho artifact areas with a median (interquartile range) of 0.035 (0.07) for the corrected spectra versus 0.18 (0.32) for the uncorrected spectra. In addition, the Cho subtraction artifacts are smaller in the corrected spectra than the uncorrected spectra in the majority of the voxels affected by the motion compensation algorithm (~84%). This improvement in spectral quality can also be seen in the unsubtracted spectra (supporting Fig. 4).

For the GSH-edited MRSI acquisition, a replacement-only motion compensation strategy was used since the water peak is saturated by the 4.56 ppm editing pulse which makes the peak more unreliable for phasing purposes. Fig. 4 shows representative uncorrected and corrected GSH.

Spectra taken from a voxel in one subject. Significant subtraction artifacts are apparent in the uncorrected spectra, but these are largely removed by the compensation algorithm allowing a clean GSH peak at 2.95 ppm to be visualized.

Fig. 5 shows represented GABA+/H_2O and GSH/H_2O maps with and without motion compensation. Both the GABA + map and the GSH maps become smoother after the motion compensation algorithm is applied, especially at the central regions of the brain.

Table 1
Phase corrections and replacements made by the motion compensation algorithm for each subject.

Subject	Number of transients phased	Transient absolute phase correction (degrees)	Number of transients replaced	Number of k-space points replaced with zeros
1	79	38	39	0
2	58	39	24	1
3	97	40	39	0
4	93	49	38	1
5	90	46	29	1
6	85	35	33	0
7	67	40	23	0
8	58	39	24	1
Median	82	39.5	31	0.5
Interquartile Range	29	4.5	14.5	1

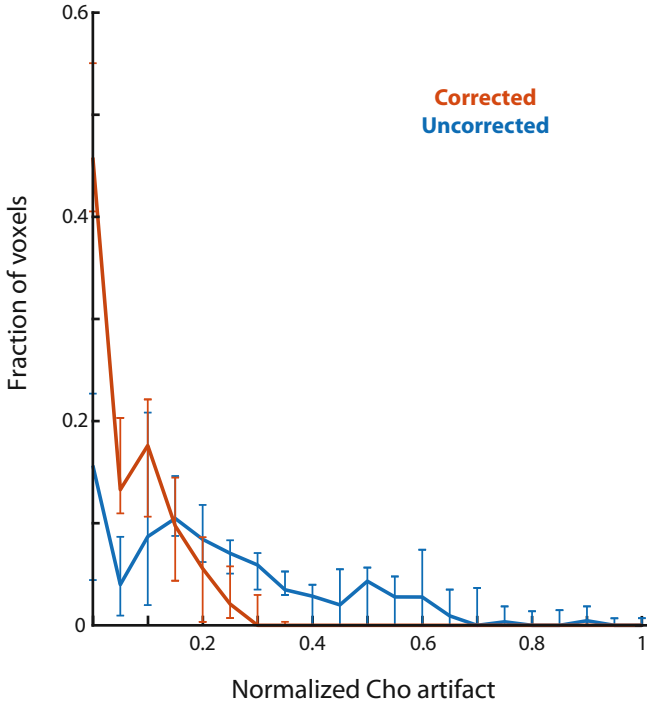

Fig. 3. Cho subtraction artifacts resulting from fits to the GABA-edited data as in supplemental Fig. 3. Median distribution and interquartile range of the Cho subtraction artifacts across all subjects. The distribution of the Cho subtraction artifacts for the corrected spectra is skewed towards lower values versus that of the uncorrected spectra.

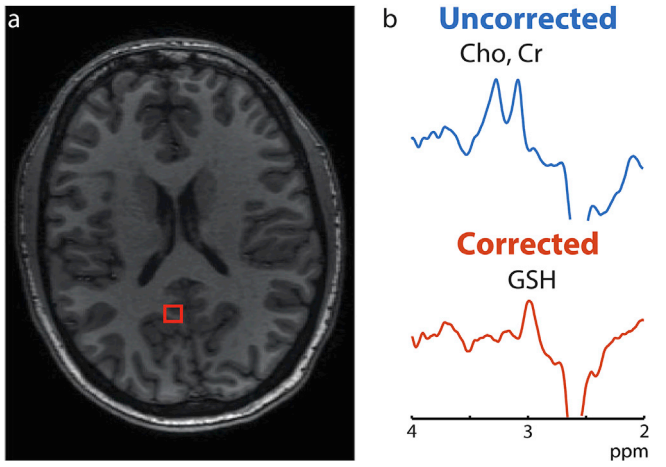

Fig. 4. Representative GSH uncorrected and corrected spectra from a voxel within this slice location is shown on the right plotted from 2 to 4 ppm. Large Cho and Cr subtraction artifacts can be seen in the uncorrected spectra, which are removed after compensation allowing visualization of the GSH peak at 2.95 ppm.

4. Discussion

The sensitivity of edited MR spectroscopic imaging to head motion necessitates the availability of accessible motion compensation methods to improve the accuracy and reliability of measurements. This paper presents a retrospective motion compensation algorithm for edited MRSI. This compensation does not require any additional hardware or acquisitions, and only requires additional data post-processing. In addition, this technique is data-based and does not rely on any assumptions about the data which could potentially lead to the introduction of artifacts upon compensation. The technique presented here is shown to be effective in significantly reducing subtraction artifacts in GABA-edited MRSI acquisitions and to have potential in correcting for motion in GSH-edited MRSI acquisitions. Although shown here to be effective in correcting edited MRSI acquisitions with Cartesian-based k-space sampling, this method can also be extended to other edited MRSI acquisitions with different k-space sampling techniques such as spiral-based trajectories or zig-zag transversal of k-space with echo planar spectroscopic imaging provided that at least 2 transients exist for each sub-acquisition type (at least 2 ONs and 2 OFFs). While additional frequency correction for B_0 drift was not necessary for the data collected here, this can be a future addition to the presented algorithm.

It is noted that both the GABA+ and GSH maps contain an asymmetry in the edited signal intensities in the left-right direction. It is believed that this originates from residual field inhomogeneity with large measurement volumes such as the one used in this study. This results in residual lipid signals which bias measurements.

Retrospective motion compensation in this study is made possible by the acquisition of multiple transients of the same type of sub-acquisition with the same phase-encoding gradient. For accurate phase compensation at a particular k-space point, at least 2 of the transients must be similar for the algorithm to phase the other transients to. If the program is unable to phase the transients and must replace a motion-corrupted transient, one of those two transients must be of the same sub-type. Thus, for a 4-transient acquisition, the two similar transients must be of different subtypes. However, the program preferentially chooses to preserve as many transients as possible with phase-correcting rather than replacing transients to reduce the amount of SNR loss resulting from replacing transients which results in an increase in the noise level relative to the signal level. However, it is possible that this SNR loss will be increased in acquisitions where more transients are removed with more severe head movements. Replacing all transients with zeros at certain k-space points was avoided as much as possible, as removing too many k-space points will degrade the MRSI point spread function and lead to artifacts.

For effective retrospective motion compensation, a reliably large residual water peak was necessary for identifying and correcting motion-affected transients. In this study, the HGDB dual water and lipid suppression sequence gave sufficient suppression factors to allow for the detection of the metabolite peaks, but also provided a reliable residual water peak for retrospective motion compensation as it originated from the entire slice. This is likely to be possible as well with other water suppression techniques such as WET (Ogg et al., 1994) or with water-suppression cycling (Ernst and Li, 2011) provided that a large enough water peak is available for correction. This is essential for GSH-edited acquisitions where the water peak at 4.68 ppm is saturated by the ON-editing pulse at 4.56 ppm. The reduced intensity of the residual water peak makes phase correction less reliable but is sufficient for identifying movement-affected transients. Thus, a replacement-only approach was used for the GSH-edited data, which can result in a reduction in SNR. Phase correction can be added, however, with the use of a weaker water suppression method which would allow for a more reliable water peak for phasing.

Accurate phasing becomes more difficult at outer k-space regions due to the lower SNR available. These points, however, also contribute less to MRSI signal after Fourier transformation, so that small phase errors on these points are relatively less important. It is important to note,

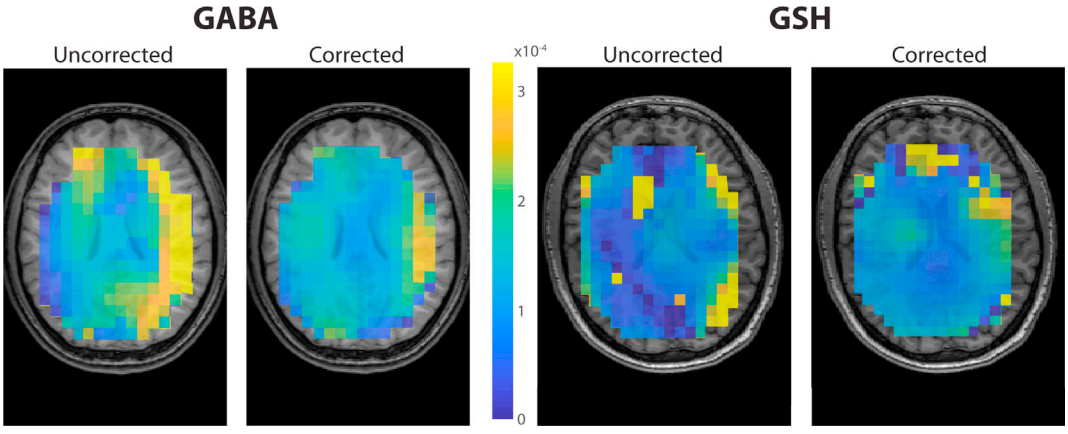

Fig. 5. Representative GABA+/H_2O and GSH/H_2O maps with and without motion compensation. Motion compensation removes much of the artifacts present in the metabolic maps and results in smoother GABA+ and GSH maps across the brain.

however, that with more severe head motion, more transients will be unrecoverable by phase correction and the SNR will likely decrease further. With a more reliable water peak for phasing, however, it is hopeful that the need for transient replacement as well as any associated SNR decreases will be kept to a minimum. Additionally, this compensation technique can be extended to also incorporate phase and frequency compensation resulting from B_0 drift during the scan and some rarely used decisions made by the algorithm can be improved upon or combined for a more streamlined approach.

In this study, a repetition time of 2s was sufficiently long enough so that moderate motion would not affect sequential transients at the same k-space point. As the repetition time decreases, however, it is possible that some movements would affect more than 2 of the 4 transients at the same k-space point which would make it difficult to find a motion-uncorrected transient. This can be mitigated by interleaving k-space transients to reduce the number of transients at the same k-space point corrupted by motion.

Although the algorithm is able to compensate for intermittent motion, the algorithm is more limited when it comes to other types of motion as seen in supporting Fig. 5. With continuous motion, the performance of the algorithm is variable. If at least one ON and one OFF are not affected by motion, the algorithm is able to phase correct or replace the motion-affected transients. If this is not the case, however, the algorithm is either unable to correct the motion-affected transients or zeroes out the point in k-space. This is also the case with frequent motion as there aren't enough unaffected transients at any given k-space point to correct for motion. The algorithm is also unable to compensate for a persistent pose change during the scan.

As noted above, methods exist for prospective motion correction for edited-MRSI acquisitions by acquiring a volumetric navigator each TR and performing real-time shim and motion compensation (Bogner et al., 2014a, 2014b). These techniques however do require software (and also hardware, if optical detection of motion is performed) that at the current time is not widely available in the MR community. In addition, the time to perform the volume navigator acquisition and online processing is long (~760 ms) (Bogner et al., 2014b) and may put a restriction on the minimum repetition time for fast MRSI sequences such as multi-slice acquisitions.

5. Conclusion

In summary, a retrospective motion compensation for edited MR spectroscopic imaging was proposed and evaluated. The method doesn't require additional hardware or additional scan time making it suitable for implementation with J-difference MR spectroscopic imaging sequences that acquire more than one transient per point in k-space. The method is expected to work best when there are intermittent subject movements after which the subjects resumes the same head position, and is not intended for use when motion is more frequent and/or larger amplitude; in these cases, full prospective motion correction will be needed (Bogner et al., 2014b).

Acknowledgments

This work was supported by NIH P41 EB015909.

Appendix A. Supplementary data

Supplementary data to this article can be found online at https://doi.org/10.1016/j.neuroimage.2019.116141.

References

Bogner, W., Gagoski, B., Hess, A.T., et al., 2014. 3D GABA imaging with real-time motion correction, shim update and reacquisition of adiabatic spiral MRSI. Neuroimage 103, 290–302.

Bogner, W., Hess, A.T., Gagoski, B., Tisdall, M.D., van der Kouwe, A.J.W., Trattnig, S., Rosen, B., Andronesi, O.C., 2014. Real-time motion- and B0-correction for LASER-localized spiral-accelerated 3D-MRSI of the brain at 3T. Neuroimage 88, 22–31.

Chan, K.L., Oeltzschner, G., Schär, M., Barker, P.B., Edden, R.A.E., 2017. Spatial Hadamard encoding of J -edited spectroscopy using slice-selective editing pulses. NMR Biomed. e3688.

Chan, K.L., Oeltzschner, G., Saleh, M.G., Edden, R.A.E., Barker, P.B., 2019. Simultaneous editing of GABA and GSH with Hadamard-encoded MR spectroscopic imaging. Magn. Reson. Med. 82, 21–32.

Chang, L., Cloak, C.C., Ernst, T., 2003. Magnetic resonance spectroscopy studies of GABA in neuropsychiatric disorders. J. Clin. Psychiatry 64, 7–14.

Choi, C., Zhao, C., Dimitrov, I., Douglas, D., Coupland, N.J., Kalra, S., Hawesa, H., Davis, J., 2009. Measurement of glutathione in human brain at 3T using an improved double quantum filter in vivo. J. Magn. Reson. 198, 160–166.

Dharmadhikari, S., Ma, R., Yeh, C., Stock, A., Snyder, S., Zauber, S.E., Dydak, U., Beste, C., 2015. NeuroImage Striatal and thalamic GABA level concentrations play differential roles for the modulation of response selection processes by proprioceptive information. Neuroimage 120, 36–42.

Do, K.Q., Cuenod, M., Hensch, T.K., 2018. Targeting Oxidative Stress and Aberrant Critical Period Plasticity in the Developmental Trajectory to Schizophrenia, vol 41, pp. 835–846.

Edden, R.A.E., Schär, M., Hillis, A.E., Barker, P.B., 2006. Optimized detection of lactate at high fields using inner volume saturation. Magn. Reson. Med. 56, 912–917.

Edden, R.A.E., Puts, N.A.J., Harris, A.D., Barker, P.B., Evans, C.J., 2014. Gannet: a batch-processing tool for the quantitative analysis of gamma-aminobutyric acid-edited MR spectroscopy spectra. J. Magn. Reson. Imaging 1452, 1445–1452.

Ernst, T., Li, J., 2011. A novel phase and frequency navigator for proton magnetic resonance spectroscopy using water-suppression cycling. Magn. Reson. Med. 65, 13–17.

Evans, C.J., Puts, N.A.J., Robson, S.E., Boy, F., Mcgonigle, D.J., Sumner, P., Singh, K.D., Edden, R.A.E., 2013. Subtraction Artifacts and Frequency (Mis-) Alignment in J -Difference GABA Editing, vol 975, pp. 970–975.

Gruetter, R., 1993. Automatic, localized in Vivo adjustment of all first- and second-order shim coils. Magn. Reson. Med. 29, 804–811.

Harris, A.D., Saleh, M.G., Edden, R.A.E., 2017. Edited 1 H Magnetic Resonance Spectroscopy in Vivo: Methods and Metabolites, vol 1389, pp. 1377–1389.

Henning, A., Fuchs, A., Murdoch, J.B., Boesiger, P., 2009. Slice-selective FID Acquisition, Localized by Outer Volume Suppression (FIDLOVS) for 1H-MRSI of the Human Brain at 7 T with Minimal Signal Loss, vol 22, pp. 683–696.

Henry, P.G., Dautry, C., Hantraye, P., Bloch, G., 2001. Brain GABA editing without macromolecule contamination. Magn. Reson. Med. 45, 517–520.

Isaacson, J.S., Scanziani, M., 2011. How inhibition shapes cortical activity. Neuron 72, 231–243.

Jocham, G., Hunt, L.T., Near, J., Behrens, T.E.J., 2012. A mechanism for value- guided choice based on the excitation-inhibition balance in prefrontal cortex. Nat. Neurosci. 15, 960–961.

Mao, X., Jiang, C.S., Kang, G., Milrad, S., Mcewen, B.S., Krieger, A.C., Shungu, D.C., 2017. Dorsolateral prefrontal cortex GABA deficit in older adults with sleep-disordered breathing. Proc. Natl. Acad. Sci. 114. E9424–E9424.

Matsuzawa, D., Obata, T., Shirayama, Y., et al., 2008. Negative correlation between brain glutathione level and negative symptoms in schizophrenia: a 3T 1H-MRS study. PLoS One 3, e1944.

Mullins, P.G., Mcgonigle, D.J., Gorman, R.L.O., Puts, N.A.J., Vidyasagar, R., Evans, C.J., Symposium, C., Edden, R.A.E., 2014. NeuroImage Current practice in the use of MEGA-PRESS spectroscopy for the detection of GABA. Neuroimage 86, 43–52.

Mytilineou, C., Kramer, B.C., Yabut, J.A., 2002. Glutathione depletion and oxidative stress. Park. Relat. Disord. 8, 385–387.

Near, J., Edden, R., Evans, C.J., Harris, A., Jezzard, P., 2015. Frequency and phase drift correction of magnetic resonance spectroscopy data by spectral registration in the time domain. Magn. Reson. Med. 50, 44–50.

Ogg, R.J., Kingsley, R.B., Taylor, J.S., 1994. WET, a T1- and B1-insensitive water-suppression method for in vivo localized 1H NMR spectroscopy. J. Magn. Reson. Ser. B 104, 1–10.

Petroff, O.A.C., 2002. GABA and Glutamate in the Human Brain, pp. 562–573.

Puts, N.A.J., Edden, R.A.E., 2012. In vivo magnetic resonance spectroscopy of GABA: a methodological review. Prog. Nucl. Magn. Reson. Spectrosc. 60, 29–41.

Schulz, J.B., Lindenau, J., Seyfried, J., Dichgans, J., 2000. Glutathione, oxidative stress and neurodegeneration. Eur. J. Biochem. 267, 4904–4911.

Shetty, A.K., Bates, A., 2016. Potential of GABA-ergic cell therapy for schizophrenia , neuropathic pain , and Alzheimer's and Parkinson's diseases. Brain Res. 1638, 74–87.

Srinivasan, R., Ratiney, H., Hammond-Rosenbluth, K.E., Pelletier, D., Nelson, S.J., 2010. MR spectroscopic imaging of glutathione in the white and gray matter at 7 T with an application to multiple sclerosis. Magn. Reson. Imaging 28, 163–170.

Tapper, S., Tisell, A., Helms, G., Lundberg, P., 2019. Retrospective artifact elimination in MEGA-PRESS using a correlation approach. Magn. Reson. Med. 81, 2223–2237.

Trabesinger, A., Weber, O., Duc, C., Boesiger, P., 1999. Detection of glutathione in the human brain in vivo by means of double quantum coherence filtering. Magn. Reson. Med. 42 (2), 283–289.

Waddell, K.W., Avison, M.J., Joers, J.M., Gore, J.C., 2007. A Practical Guide to Robust Detection of GABA in Human Brain by J -difference Spectroscopy at 3 T Using a Standard Volume Coil, vol 25, pp. 1032–1038.

Weiduschat, N., Mao, X., Hupf, J., Armstrong, N., Kang, G., Lange, D.J., Mitsumoto, H., Shungu, D.C., 2014. Motor cortex glutathione deficit in ALS measured in vivo with the J-editing technique. Neurosci. Lett. 570, 102–107.

Wiegers, E.C., Philips, B.W.J., Heerschap, A., van der Graaf, M., 2017. Automatic frequency and phase alignment of in vivo J-difference- edited MR spectra by frequency domain correlation. Magma 30, 537–544.
Wood, S.J., Berger, G.E., Wellard, R.M., Proffitt, T.-M., McConchie, M., Berk, M., McGorry, P.D., Pantelis, C., 2009. Medial temporal lobe glutathione concentration in first episode psychosis: a 1H-MRS investigation. Neurobiol. Dis. 33, 354–357.
Zhu, H., Ouwerkerk, R., Barker, P.B., 2010. Dual-band water and lipid suppression for MR spectroscopic imaging at 3 tesla. Magn. Reson. Med. 63, 1486–1492.
Zhu, H., Edden, R.A.E., Ouwerkerk, R., Barker, P.B., 2011. High resolution spectroscopic imaging of GABA at 3 tesla. Magn. Reson. Med. 65, 603–609.